Available online at www.sciencedirect.com
SCIENCE DIRECT
Journal of Sound and Vibration 291 (2006) 802–823
JOURNAL OF SOUND AND VIBRATION
www.elsevier.com/locate/jsvi

A shear beam finite element for the damping analysis of tubular laminated composite beams

D.A. Saravanos*, D. Varelis, T.S. Plagianakos, N. Chrysochoidis

Department of Mechanical Engineering & Aeronautics, University of Patras, Patras 26500, Greece

Received 21 January 2004; received in revised form 9 June 2005; accepted 28 June 2005
Available online 18 January 2006

Abstract

The paper presents a three-dimensional beam element developed for predicting the damping of composite blades with hollow laminated cross-sections. The unified theoretical framework for synthesizing the equivalent damping properties of a tubular composite blade section is outlined. Building upon the damping mechanics, a damped three-dimensional shear beam finite element is developed, which explicitly provides damping, stiffness and mass matrices. A methodology for analyzing the damped free-vibration response of tubular beams is formulated, and modal frequencies and modal damping values are predicted. Application examples illustrate the ability of the beam element to predict the modal damping and modal frequencies of hollow blades of various uniform circular, elliptical and box sections. The results further quantify the ability of the element to capture the strong effect of skin laminations, as well as the contribution of shear to the modal damping of the beam.

1. Introduction

The continuous evolution of wind-turbine and helicopter rotors towards longer and more flexible composite blade configurations and the associated implications on blade aero-elastic performance and fatigue life, are placing new requirements for understanding, analyzing and possibly improving the passive damping which composite materials introduce into a tubular composite blade structure. These requirements call, among other issues, for the development of admissible theoretical frameworks and analytical capabilities which in the long term will enable simultaneous predictions of damping, stiffness and mass in composite blades, while understanding the effect of various material and geometry parameters on structural damping. In order to cover this void in current analytical and modeling technology, novel integrated composite damping mechanics and a new finite element for tubular composite beams have been developed, for the prediction of the damped free-vibration response using minimal input of material and geometrical parameters. This paper outlines the theoretical background of a new shear-deformable damped beam finite element and illustrates its capability to predict the structural modal damping of composite blades.

*Corresponding author. Tel.: +30 2610 996191; fax: +30 2610 992644.
E-mail address: saravanos@mech.upatras.gr (D.A. Saravanos).

0022-460X/$ - see front matter © 2005 Elsevier Ltd. All rights reserved.
doi:10.1016/j.jsv.2005.06.045

Most of the reported work in the area of composite damping modeling has been focused on damping mechanics of composite materials and laminates [1–4]. Various analytical solutions and finite elements for predicting the damping of laminated plate and shell structures have been also reported [5–10]. On the other hand, various composite beam formulations and finite elements for predicting the static and undamped dynamic response of composite blades have been also developed [11–19]. However, no work seems to have been reported towards the development of beam mechanics and finite elements capable of predicting the damping of tubular composite blades.

In the following sections, damping mechanics developed for predicting the equivalent damping of tubular laminated composite beam sections of arbitrary geometry are briefly described. The formulation includes multi-scale damping models for each composite ply, for the skin laminate, and eventually for the complete tubular beam section. The beam kinematics entail constant shear assumptions, thus the beam damping mechanics include effects of transverse shear on both beam damping and stiffness. Based on this damped beam model, a three-dimensional shear beam finite element is subsequently formulated for predicting the structural damping of hollow composite beams and blades. In the present formulation, emphasis is mainly placed on skin laminations exhibiting negligible extension–shear coupling. Through the integrated approach, the finite element has the capability to yield damping matrices, in addition to stiffness and mass matrices, which are explicitly related to a minimal number of input parameters, such as, the damping and elastic coefficients of the composite material, the skin laminate configurations, the cross-section shape and the overall blade geometry. The capability of the new element to effectively predict modal damping and frequencies of typical composite beam configurations is quantified next, through a series of evaluation and validation cases. The numerical results also illustrate the combined effect of composite materials, skin lamination, cross-sectional configuration and beam geometry on the overall structural damping and the natural frequencies of the beam.

2. Tubular laminated beam

This section provides a brief description of the damped beam mechanics of beams having a hollow tubular laminated cross-section, as the one shown in Fig. 1. It is assumed that the section is closed, has an arbitrary geometry and that the skin may consist of various segments of arbitrary lamination which are defined about its mid-line. The beams are assumed to be neither curved nor pre-twisted. The equivalent cross-section properties are expressed in terms of a Cartesian coordinate system *Oxyz*; whereas, the skin lamination, ply properties and

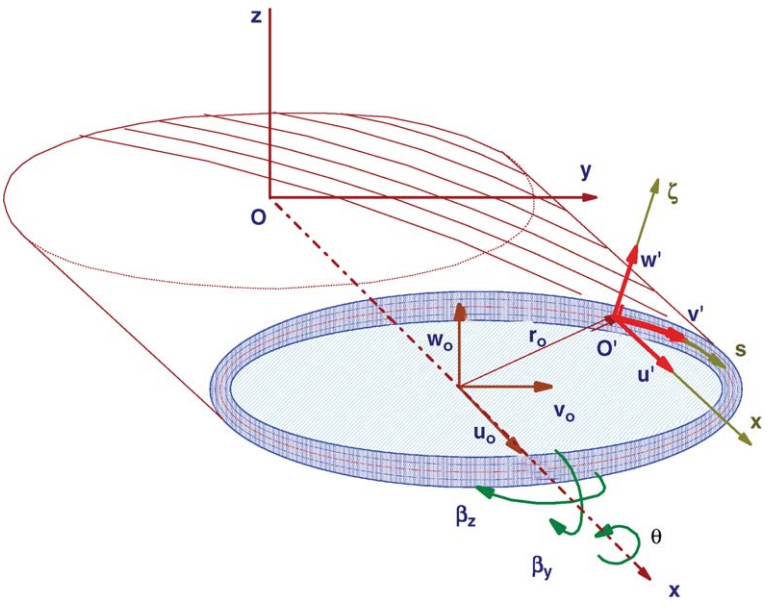

Fig. 1. Typical hollow beam cross-section geometry, coordinate systems and generalized displacements.

equivalent properties of the skin laminate are defined in terms of the local curvilinear system $Oxs\zeta$ shown in Fig. 1. The assumed positive directions of generalized displacements and equivalent forces and moments are also shown in Fig. 1.

2.1. Section kinematics

The assumed section deformation admits extension along x-axis, bending in y and z directions, torsion about the x-axis and shear deformation in y and z directions. In this context, it is reasonable to assume that at each point of the skin laminate the equivalent transverse normal and shear laminate stresses N_{ss}, $N_{s\zeta}$, and transverse moment M_s defined along the local coordinate system $O'xs\zeta$, should be negligible. Moreover, the displacements at each point of the section are expressed in the Cartesian system $Oxyz$ by the following equations:

$$u(x,y,z) = u^0(x) + \beta_y(x)z + \beta_z(x)y + \theta_{,x}(x)\Psi(y,z),$$

$$v(x,y,z) = v^0(x) - \theta(x)z,$$

$$w(x,y,z) = w^0(x) + \theta(x)y, \tag{1}$$

where u^0, v^0, w^0 are the displacements of the section at the origin of the coordinate system $Oxyz$; β_y, β_z are bending rotation angles about axes y and z, respectively; θ is the twisting angle and $\Psi(y,z)$ is the secondary warping of the section; the comma in the subscripts indicates differentiation. In the curvilinear system $O'xs\zeta$, kinematic assumptions (1) are expressed by the following form:

$$u'(x,s,\zeta) = u^0(x) + \beta_y(x)(z_0 + y^0_{,s}\zeta) + \beta_z(x)(y_0 - z^0_{,s}\zeta) + \theta_{,x}(x)(-r^0_\zeta\zeta + \Psi^0(s)),$$

$$v'(x,s,\zeta) = v^0(x) - \theta(x)(r^0_\zeta + \zeta),$$

$$w'(x,s,\zeta) = w^0(x) + \theta(x)r^0_s, \tag{2}$$

where (y^0, z^0) and (r^0_s, r^0_ζ) are the projections of the vector $\mathbf{r}^0$ describing the distance between a point O' on the skin mid-surface from point O on the section axis x, on the respective axes of coordinate systems $Oxyz$ and $O'xs\zeta$; $\Psi(s,\zeta) = -r^0_\zeta\zeta + \Psi^0(s)$ is the secondary warping function of the section. The prime symbol indicates vector and tensor components expressed in the curvilinear system, and is implied in the following paragraphs. The assumed section deformation yields the normal and shear strains acting on the cross-section

$$\varepsilon_x(x,s,\zeta) = \varepsilon^0_x(x) + k_{xy}(x)(z_0 + y^0_{,s}\zeta) + k_{xz}(x)(y_0 - z^0_{,s}\zeta) + \theta_{,xx}(x)(-r^0_\zeta\zeta + \Psi^0(s)),$$

$$\varepsilon_{xs}(x,s,\zeta) = \varepsilon^0_{xz}(x)z^0_{,s} + \varepsilon^0_{xy}(x)y^0_{,s} + \varepsilon^{0t}_{xs}(x,s) - 2\theta_{,x}\zeta,$$

$$\varepsilon_{x\zeta}(x,s,\zeta) = \varepsilon^0_{xz}(x)y^0_{,s} - \varepsilon^0_{xy}(x)z^0_{,s}. \tag{3}$$

In the above equations, the generalized strains, which equivalently describe the deformation of the section, include the axial strain ε^0_x, the transverse shear strains $\varepsilon^0_{xy}, \varepsilon^0_{xz}$, the bending curvatures k_{xy}, k_{xz} and the twisting curvatures k_θ, $k_{\theta\theta}$, where

$$\varepsilon^0_x = u^0_x, \quad \varepsilon^0_{xy} = v^0_{,x} + \beta_z, \quad \varepsilon^0_{xz} = w^0_{,x} + \beta_y,$$

$$k_{xy} = \beta_{y,x}, \quad k_{xz} = \beta_{z,x}, \quad k_\theta = \theta_{,x}, \quad k_{\theta\theta} = \theta_{,xx}. \tag{4}$$

The second twisting curvature $k_{\theta\theta}$ expresses second-order variation and is assumed to be negligible with respect to the other generalized strains. The torsional strain on the mid-surface $\varepsilon^0_{xs}t$ can be evaluated by considering and solving the torsion stress equilibrium equation on the $s\zeta$ plane using a properly chosen torsional strain function Φ. In this context, the mid-surface torsional strain and the secondary warping

function are found to be

$$\varepsilon_{xs}^{0t}(s) = \Delta\Phi(s)/h(s),$$

$$\Psi^0(s) = \Delta A_0 - \frac{\Delta\Phi}{\theta_{,x}}\,\Delta\lambda, \tag{5}$$

where $\Delta\Phi$ is the difference of the strain function between the inner and outer surface, A_0 and λ are geometric section parameters defined by

$$\frac{\Delta\Phi(s)}{\theta_{,x}} = -A_0/\lambda,$$

$$\Delta A_0 = \int_0^s r_\zeta^0\,\mathrm{d}s, \quad \Delta\lambda = \int_0^s \frac{1}{h}\,\mathrm{d}s, \quad A_0 = \oint r_\zeta^0\,\mathrm{d}s, \quad \lambda = \oint \frac{1}{h}\,\mathrm{d}s. \tag{6}$$

2.2. Equations of motion

The equations of motion of the beam can be described by a variational form,

$$\int_0^l \mathrm{d}x \int_A (-\delta H + \delta T - \delta W_d)\,\mathrm{d}s\,\mathrm{d}\zeta + \oint_\Gamma \delta\bar{u}_i^{\mathrm{T}}\bar{\tau}\,\mathrm{d}\Gamma = 0, \tag{7}$$

where δH and δT are the strain and kinetic energy variations, δW_d is the variation in dissipated energy, τ overbar is surface traction on the free surface Γ, A is the cross-sectional area covered by the material, and l the length of the beam. The variation of the strain and kinetic energy of the section are represented by the respective integrals over the cross-sectional area.

$$\delta H_s = \int_A \delta\boldsymbol{\varepsilon}_c^{\mathrm{T}}\boldsymbol{\sigma}_c\,\mathrm{d}s\,\mathrm{d}\zeta = \oint \mathrm{d}s \int_h (\delta\varepsilon_x\,\sigma_x + \delta\varepsilon_{xs}\,\sigma_{xs} + \delta\varepsilon_{x\zeta}\,\sigma_{x\zeta})\,\mathrm{d}\zeta = \oint \mathrm{d}s \int_h \delta\boldsymbol{\varepsilon}_c^{\mathrm{T}}[Q_c]\boldsymbol{\varepsilon}_c\,\mathrm{d}\zeta,$$

$$\delta T_s = \int_A -\delta\mathbf{u}^{\mathrm{T}}\,\mathbf{diag}(\boldsymbol{\rho})\ddot{\mathbf{u}}\,\mathrm{d}\xi\,\mathrm{d}\eta = \oint \mathrm{d}s \int_h -(\delta u\,\rho\ddot{u} + \delta v\,\rho\ddot{v} + \delta w\,\rho\ddot{w})\,\mathrm{d}\zeta, \tag{8}$$

where $\mathbf{diag}(\boldsymbol{\rho})$ indicates a diagonal matrix with diagonal elements equal to the mass density ρ of a ply. The dissipated strain energy of the cross-section due to viscoelastic damping during harmonic motion is given by

$$\delta W_{ds} = \int_A \delta\boldsymbol{\varepsilon}_c^{\mathrm{T}}\boldsymbol{\eta}_c\mathbf{Q}_c\boldsymbol{\varepsilon}_c\,\mathrm{d}s\,\mathrm{d}\zeta = \oint \mathrm{d}s \int_h \delta\boldsymbol{\varepsilon}_c^{\mathrm{T}}\boldsymbol{\eta}_c\mathbf{Q}_c\boldsymbol{\varepsilon}_c\,\mathrm{d}\zeta. \tag{9}$$

In the above equations, $\boldsymbol{\varepsilon}_c = \{\varepsilon_{c1}, \varepsilon_{c5}, \varepsilon_{c6}\} = \{\varepsilon_{cx}, \varepsilon_{cx\zeta}, \varepsilon_{cxs}\}$ and $\boldsymbol{\sigma}_c = \{\sigma_{c1}, \sigma_{c5}, \sigma_{c6}\} = \{\sigma_{cx}, \sigma_{cx\zeta}, \sigma_{cxs}\}$ are the off-axis strains and stresses of a composite ply; $\mathbf{Q}_c$ and $\boldsymbol{\eta}_c$ are equivalent off-axis stiffness and damping (loss-factor) matrices of a composite ply with respect to the system $Oxs\zeta$, defined in the appendix; h is the thickness of the skin laminate.

2.3. Equivalent section stiffness

Using the strain expressions provided by Eq. (3) into Eq. (8), integrating over the thickness first, and then around the skin midline, the stored strain energy of the section is expressed in terms of the generalized section strains and the equivalent section stiffness terms, as follows:

$$\delta H_s = \oint (\delta\boldsymbol{\varepsilon}^{0^{\mathrm{T}}}\mathbf{A}^0\boldsymbol{\varepsilon}^0 + 2\delta\boldsymbol{\varepsilon}^{0^{\mathrm{T}}}\mathbf{B}^0\mathbf{k} + \delta\mathbf{k}^{\mathrm{T}}\mathbf{D}^0\mathbf{k})\,\mathrm{d}s, \tag{10}$$

where $\boldsymbol{\varepsilon}^0 = \{\varepsilon_x^0, \varepsilon_{x\zeta}^0, \varepsilon_{xs}^0\}$ and $\mathbf{k} = \{k_{xy}, k_{xz}, k_\theta\}$ represent the average strains and curvatures of the section, respectively. $\mathbf{A}^0, \mathbf{B}^0, \mathbf{D}^0$ are the resultant equivalent extensional–shear, coupling and flexure–torsional stiffness

matrices of the cross-section, having the form

$$\mathbf{A}^0 = \begin{bmatrix} A^0_{11} & \bar{A}^0_{15} & \bar{A}^0_{16} \\ \bar{A}^0_{51} & A^0_{55} & A^0_{56} \\ \bar{A}^0_{61} & A^0_{65} & A^0_{66} \end{bmatrix}, \quad \mathbf{B}^0 = \begin{bmatrix} B^0_{11} & B^0_{12} & \bar{B}^0_{16} \\ \bar{B}^0_{51} & \bar{B}^0_{52} & B^0_{56} \\ \bar{B}^0_{61} & \bar{B}^0_{62} & B^0_{66} \end{bmatrix}, \quad \mathbf{D}^0 = \begin{bmatrix} D^0_{11} & D^0_{12} & \bar{D}^0_{16} \\ D^0_{21} & D^0_{22} & \bar{D}^0_{26} \\ \bar{D}^0_{61} & \bar{D}^0_{62} & D^0_{66} \end{bmatrix}. \tag{11}$$

In the previous equations the extensional and shear stiffness terms are found to be given by

$$A^0_{11} = \oint A_{11}\,\mathrm{d}s,$$

$$A^0_{15} = \oint (A_{16} z^0_{,s})\,\mathrm{d}s,$$

$$A^0_{16} = \oint (A_{16} y^0_{,s})\,\mathrm{d}s,$$

$$A^0_{55} = \oint (A_{66} z^{0^2}_{,s})\,\mathrm{d}s + \oint (A_{55} y^{0^2}_{,s})\,\mathrm{d}s,$$

$$A^0_{56} = \oint (A_{66} z^0_{,s} y^0_{,s})\,\mathrm{d}s + \oint (A_{55} y^0_{,s} z^0_{,s})\,\mathrm{d}s,$$

$$A^0_{66} = \oint (A_{66} y^{0^2}_{,s})\,\mathrm{d}s + \oint (A_{55} z^{0^2}_{,s})\,\mathrm{d}s, \tag{12}$$

the flexural and torsional terms are

$$D^0_{11} = \oint (A_{11} z^{0^2} + 2 z^0 y^0_{,s} B_{11} + y^{0^2}_{,s} D_{11})\,\mathrm{d}s,$$

$$D^0_{12} = D^0_{21} = \oint (A_{11} z^0 y^0 + (y^0 y^0_{,s} - z^0 z^0_{,s}) B_{11} - y^0_{,s} z^0_{,s} D_{11})\,\mathrm{d}s,$$

$$D^0_{16} = \oint (-A_h z^0 A_{16} - (A_h y^0_{,s} + 2 z^0) B_{16} - 2 y^0_{,s} D_{16})\,\mathrm{d}s,$$

$$D^0_{22} = \oint (A_{11} y^{0^2} - 2 z^0_{,s} y^0 B_{11} + z^{0^2}_{,s} D_{11})\,\mathrm{d}s,$$

$$D^0_{26} = \oint (-A_h y^0 A_{16} + (A_h z^0_{,s} - 2 y^0) B_{16} - 2 z^0_{,s} D_{16})\,\mathrm{d}s,$$

$$D^0_{66} = \oint (A^2_h + A_{66} + 4 A_h B_{66} + 4 D_{66})\,\mathrm{d}s \tag{13}$$

and the coupling terms

$$B^0_{11} = \oint (A_{11} z^0 + B_{11} y^0_{,s})\,\mathrm{d}s,$$

$$B^0_{12} = \oint (A_{11} y^0 - B_{11} z^0_{,s})\,\mathrm{d}s,$$

$$B^0_{16} = \oint (-A_{16} A_h - 2 B_{16})\,\mathrm{d}s,$$

$$B^0_{51} = \oint (A_{16} z^0 + B_{16} y^0_{,s}) z^0_{,s} \, \mathrm{d}s,$$

$$B^0_{52} = \oint (A_{16} y^0 - B_{16} z^0_{,s}) z^0_{,s} \, \mathrm{d}s,$$

$$B^0_{56} = \oint (-A_{66} A_h - 2B_{66}) z^0_{,s} \, \mathrm{d}s,$$

$$B^0_{61} = \oint (A_{16} z^0 + B_{16} y^0_{,s}) y^0_{,s} \, \mathrm{d}s,$$

$$B^0_{62} = \oint (A_{16} y^0 - B_{16} z^0_{,s}) y^0_{,s} \, \mathrm{d}s,$$

$$B^0_{66} = \oint (-A_{66} A_h - 2B_{66}) y^0_{,s} \, \mathrm{d}s. \tag{14}$$

In the above equations, $A_h = A_0/\lambda h$; $\mathbf{A}, \mathbf{B}, \mathbf{D}$ are the equivalent extensional stiffness matrices of the skin laminate defined in the appendix. The terms with overbar in Eq. (11) correspond to section stiffness terms due to extension–shear coupling in the skin laminate, and they vanish when the extension–shear, extension–torsion, and bending–torsion coupling of the skin laminate is negligible ($A_{16} = B_{16} = D_{16} = 0$). Although the study of such coupling effects is beyond the scope of the present paper, coupling terms were included in the stiffness matrices of Eq. (11) for the shake of completeness and comparison with other beam stiffness formulations.

2.4. Section mass matrices

Substituting the displacement equations (2) into the kinetic energy equation (8), and performing the integration over the thickness and around the skin midline, the kinetic energy of the section is expressed in terms of the generalized displacements and the resultant mass matrices:

$$\delta T_s = \oint (\delta \mathbf{u}^{0^{\mathrm{T}}} \mathbf{m}^{\mathbf{A}} \ddot{\mathbf{u}}^0 + 2\delta \mathbf{u}^{0^{\mathrm{T}}} \mathbf{m}^{\mathbf{B}} \ddot{\boldsymbol{\beta}} + \delta \boldsymbol{\beta}^{\mathrm{T}} \mathbf{m}^{\mathbf{D}} \ddot{\boldsymbol{\beta}}) \, \mathrm{d}s, \tag{15}$$

where $\mathbf{u}^0 = \{u^0, v^0, w^0\}$ and $\boldsymbol{\beta} = \{\beta_y, \beta_z, \theta\}$ represent the average displacements and rotations of the section, respectively; $\mathbf{m}^{\mathbf{A}}, \mathbf{m}^{\mathbf{B}}, \mathbf{m}^{\mathbf{D}}$ are the equivalent linear mass, coupling and rotational inertia matrices of the cross-section, per unit length:

$$\mathbf{m}^{\mathbf{A}} = \begin{bmatrix} m^A_{11} & 0 & 0 \\ 0 & m^A_{11} & 0 \\ 0 & 0 & m^A_{11} \end{bmatrix}, \quad \mathbf{m}^{\mathbf{B}} = \begin{bmatrix} m^B_{11} & m^B_{12} & m^B_{13} \\ 0 & 0 & m^B_{23} \\ 0 & 0 & m^B_{33} \end{bmatrix}, \quad \mathbf{m}^{\mathbf{D}} = \begin{bmatrix} m^D_{11} & m^D_{12} & m^D_{13} \\ m^D_{12} & m^D_{22} & m^D_{23} \\ m^D_{31} & m^D_{32} & m^D_{32} \end{bmatrix}. \tag{16}$$

The elements of the previous matrices are found to have the following form:

$$m^A_{11} = \oint \rho^A \, \mathrm{d}s,$$

$$m^B_{11} = \oint (z^0 \rho^A + y^0_{,s} \rho^B) \, \mathrm{d}s,$$

$$m^B_{12} = \oint (y^0 \rho^A - z^0_{,s} \rho^B) \, \mathrm{d}s,$$

$$m^B_{13} = \oint (\Psi^0 \rho^A + r^0_{\zeta} \rho^B) \, \mathrm{d}s,$$

$$m_{23}^{B} = \oint (-\rho^{A} z^{0} - \rho^{B} y_{,s}^{0})\,\mathrm{d}s,$$

$$m_{33}^{B} = \oint (\rho^{A}(-z_{,s}^{0} r_{\zeta}^{0} + y_{,s}^{0} r_{s}^{0}) - \rho^{B} z_{,s}^{0})\,\mathrm{d}s,$$

$$m_{11}^{D} = \oint (z^{0^2}\rho^{A} + 2z^{0} y_{,s}^{0}\rho^{B} + y_{,s}^{0^2}\rho^{D})\,\mathrm{d}s,$$

$$m_{12}^{D} = \oint (z^{0} y^{0}\rho^{A} + (y^{0} y_{,s}^{0} - z^{0} z_{,s}^{0})\rho^{B} - y_{,s}^{0} z_{,s}^{0}\rho^{D})\,\mathrm{d}s,$$

$$m_{13}^{D} = m_{31}^{D} = \oint (\Psi^{0} z^{0}\rho^{A} + (\Psi^{0} y_{,s}^{0} + z^{0} r_{\zeta}^{0})\rho^{B} + y_{,s}^{0} r_{\zeta}^{0}\rho^{D})\,\mathrm{d}s,$$

$$m_{22}^{D} = \oint (y^{0^2}\rho^{A} - 2y^{0} z_{,s}^{0}\rho^{B} + z_{,s}^{0^2}\rho^{D})\,\mathrm{d}s,$$

$$m_{23}^{D} = m_{32}^{D} = \oint (\Psi^{0} y^{0}\rho^{A} + (-\Psi^{0} z_{,s}^{0} + y^{0} r_{\zeta})\rho^{B} - z_{,s}^{0} r_{\zeta}\rho^{D})\,\mathrm{d}s,$$

$$m_{33}^{D} = \oint ((r_{s}^{0^2} + r_{y}^{0^2} + \Psi^{0^2})\rho^{A} + 2(r_{y}^{0} + \Psi^{0} r_{\zeta})\rho^{B} + r_{\zeta}^{2}\rho^{D})\,\mathrm{d}s. \tag{17}$$

In the above equations, $\rho^{A}, \rho^{B}, \rho^{D}$, are the equivalent average, coupling and inertia densities of the skin laminate defined in the appendix.

2.5. Beam damping

Similar to the derivation of the previous stiffness and mass relations, substituting the strain Eq. (3) into the dissipated energy equation (9) and integrating over the cross-sectional area, we arrive at the dissipated energy over a cross-section of the beam, which is expressed in terms of the generalized strains and three damping matrices:

$$\delta W_{ds} = (\delta\boldsymbol{\varepsilon}^{0^{\mathrm{T}}}\mathbf{A}_{d}^{0}\boldsymbol{\varepsilon}^{0} + \delta\boldsymbol{\varepsilon}^{0^{\mathrm{T}}}\mathbf{B}_{d}^{0}\mathbf{k} + \delta\mathbf{k}^{\mathrm{T}}\mathbf{B}_{d}^{0^{\mathrm{T}}}\boldsymbol{\varepsilon}^{0} + \delta\mathbf{k}^{\mathrm{T}}\mathbf{D}_{d}^{0}\mathbf{k}), \tag{18}$$

where W_{ds} is the dissipated energy per unit length of the beam subject to an arbitrary combination of cyclic strain bending curvatures and twisting angles. The resultant damping matrices $\mathbf{A}_{d}^{0}, \mathbf{B}_{d}^{0}, \mathbf{D}_{d}^{0}$ are new and represent the damping and energy dissipation per unit length of the beam due to extension–shear, coupling and bending–torsion deformation, respectively:

$$\mathbf{A}_{d}^{0} = \begin{bmatrix} A_{d11}^{0} & 0 & 0 \\ 0 & A_{d55}^{0} & A_{d56}^{0} \\ 0 & A_{d65}^{0} & A_{d66}^{0} \end{bmatrix}, \quad \mathbf{B}_{d}^{0} = \begin{bmatrix} B_{d11}^{0} & B_{d12}^{0} & 0 \\ 0 & 0 & B_{d56}^{0} \\ 0 & 0 & B_{d66}^{0} \end{bmatrix}, \quad \mathbf{D}_{d}^{0} = \begin{bmatrix} D_{d11}^{0} & D_{d12}^{0} & 0 \\ D_{d21}^{0} & D_{d22}^{0} & 0 \\ 0 & 0 & D_{d66}^{0} \end{bmatrix}. \tag{19}$$

In the previous equations, the extensional and shear damping terms were given by

$$A_{d11}^{0} = \oint A_{d11}\,\mathrm{d}s,$$

$$A_{d55}^{0} = \oint (A_{d66} z_{,s}^{0^2})\,\mathrm{d}s + \oint (A_{d55} y_{,s}^{0^2})\,\mathrm{d}s,$$

$$A_{d56}^{0} = A_{d65}^{0} = \oint (A_{d66} z_{,s}^{0} y_{,s}^{0})\,\mathrm{d}s + \oint (A_{d55} y_{,s}^{0} z_{,s}^{0})\,\mathrm{d}s,$$

$$A^0_{d66} = \oint (A_{d66} y^{0^2}_{,s}) \, \mathrm{d}s + \oint (A_{d55} z^{0^2}_{,s}) \, \mathrm{d}s \tag{20}$$

flexural–torsional damping terms by

$$D^0_{d11} = \oint (A_{d11} z^{0^2} + 2 z^0 y^0_{,s} B_{11} + y^{0^2}_{,s} D_{d11}) \, \mathrm{d}s,$$

$$D^0_{d12} = D^0_{d21} = \oint (A_{d11} z^0 y^0 + (y^0 y^0_{,s} - z^0 z^0_{,s}) B_{d11} - y^0_{,s} z^0_{,s} D_{d11}) \, \mathrm{d}s,$$

$$D^0_{d22} = \oint (A_{d11} y^{0^2} - 2 z^0_{,s} y^0 B_{d11} + z^{0^2}_{,s} D_{d11}) \, \mathrm{d}s,$$

$$D^0_{d66} = \oint (A_h^2 A_{d66} + 4 A_h B_{d66} + 4 D_{d66}) \, \mathrm{d}s \tag{21}$$

and coupling damping terms by

$$B^0_{d11} = \oint (A_{d11} z^0 + B_{d11} y^0_{,s}) \, \mathrm{d}s,$$

$$B^0_{d12} = \oint (A_{d11} y^0 - B_{d11} z^0_{,s}) \, \mathrm{d}s,$$

$$B^0_{d56} = \oint (-A_{d66} A_h - 2 B_{d66}) z^0_{,s} \, \mathrm{d}s,$$

$$B^0_{d66} = \oint (-A_{d66} A_h - 2 B_{d66}) y^0_{,s} \, \mathrm{d}s. \tag{22}$$

In the above equations, $\mathbf{A}_d, \mathbf{B}_d, \mathbf{D}_d$ are effective extensional, coupling and flexural loss stiffness matrices of the skin laminate defined in the appendix and were formulated by assuming negligible resultant skin laminate force and moment in the hoop direction. In the previous derivations, it was further assumed that the extension–shear, extension–torsion, and bending–torsion damping coupling of the skin laminate is negligible (i.e. $A_{d16} = B_{d16} = D_{d16} = 0$) and the corresponding damping terms were omitted in the section damping matrices (Eq. (19)) for the sake of simplicity; otherwise, these damping matrices become fully populated. Their effect of such coupling on beam damping will be included and studied in future work.

3. Damped beam element

A three-dimensional shear beam finite element was developed for the damped dynamic analysis of tubular composite beam structures (see Fig. 2), such as wind-turbine and helicopter rotor blades, robotic manipulator links and so forth. The beam finite element formulation is based on the kinematic assumptions and the shear damping beam theory formulated in the previous section. The element has 6dofs at each node (indicated with superscript i),

$$\mathbf{U}^i_e = \{u^{0i}, v^{0i}, w^{0i}, \beta^i_y, \beta^i_z, \theta^i\} \tag{23}$$

which are, respectively: the three displacements u, v, w at the origin Oyz of the section; the two bending rotation angles, and the twisting angle. The approximation of the generalized displacements along the axis of the beam are described analytically by

$$\langle u^0(x), v^0(x), w^0(x), \beta_y(x), \beta_z(x), \theta(x) \rangle \cong \sum_{i=1}^{L} N^i(x) \langle u^{0i}(x), v^{0i}(x), w^{0i}(x), \beta^i_y(x), \beta^i_y(x), \theta^i(x) \rangle, \tag{24}$$

where L is the number of nodes, $N^i(x)$ are c^0 continuous interpolation functions, and superscript i indicates nodal variables. The same interpolation functions are used for each dof. The generalized strains and

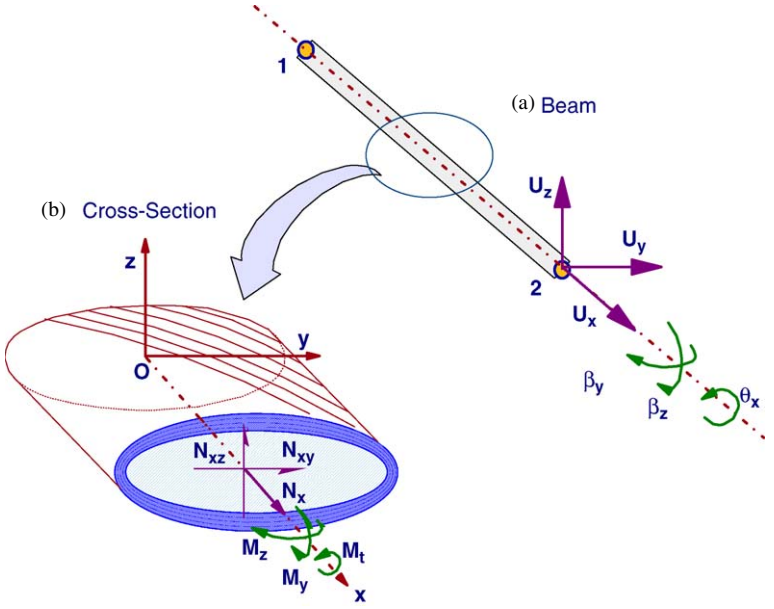

Fig. 2. Beam element and nodal degrees of freedom.

curvatures of the beam section, are now approximated using Eq. (24). By applying the previous displacement and strain approximation Eq. (24) into the equations of motion (7)–(8) and collecting the common coefficients, the stiffness and mass damping matrices of the beam finite element are formulated. Finally, after substituting Eq. (24) into Eq. (9), the element damping matrix is found to have the form

$$\mathbf{C}_e^{ij} = \int_0^l \mathbf{R}^{i^{\mathrm{T}}} \begin{bmatrix} \mathbf{A}_d^0 & \mathbf{B}_d^0 \\ \mathbf{B}_d^{0^{\mathrm{T}}} & \mathbf{D}_d^0 \end{bmatrix} \mathbf{R}^j \, \mathrm{d}x, \tag{25}$$

where the strain shape matrix $\mathbf{R}^i$ includes in-plane and shear terms, $i,j = 1,\ldots,L$. Through proper collection of the previous element matrices terms, as mandated by the equations of motion, the total stiffness $\mathbf{K}$, mass $\mathbf{M}$ and damping $\mathbf{C}$ matrices of the beam are synthesized. Assuming harmonic motion and taking into account the governing equations of motion (7)–(9), the final discrete set of equations describes the free-vibration response of the beam:

$$-\omega^2\mathbf{M}\mathbf{U} + \mathrm{j}\mathbf{C}\mathbf{U} + \mathbf{K}\mathbf{U} = \mathbf{0}. \tag{26}$$

Eq. (26) may be solved directly to yield the complex eigenvalues of the system. Alternatively, using an energy approach, numerical solution of the undamped system ($\mathbf{C} = \mathbf{0}$) provides the undamped modal frequencies and mode shapes of the beam structure, and the modal loss factors of the beam are calculated as the ratio of the respective dissipated to maximum stored modal energy, which have the form

$$\eta_m = \frac{1}{2\pi} \frac{\mathbf{U}_m^{\mathrm{T}}\mathbf{C}\mathbf{U}_m}{\mathbf{U}_m^{\mathrm{T}}\mathbf{K}\mathbf{U}_m}, \tag{27}$$

where $\mathbf{U}_m$ is the mode deflection. Using the previous described formulation, a beam element with $L = 2$ nodes and linear shape functions was developed and encoded into a research code named DAMPBEAM, which predicts the damped dynamic characteristics (natural frequencies, modal damping and mode shapes) of the beam model.

4. Results and discussion

The developed damped beam mechanics and finite element were evaluated by predicting the modal damping and modal frequency values of glass/polyester plate beams, tubular beams of circular section, and hollow elliptical and rectangular-box section blades (Fig. 3). Unless otherwise stated, in all cases the results were predicted using 20 uniformly spaced beam elements. Whenever applicable, obtained numerical results were compared with numerical results obtained using a previously developed shell damping mechanics theory and an eight-node composite shell finite element [10]. The damping coefficients, mechanical properties and nominal ply thickness of the glass/polyester composite material used in this work are shown in Table 1, and correspond to experimentally measured values [20]. In all cases the skin laminations are described in standard laminate notation, with first ply taken at the inner surface of the skin.

The capability of the present method to predict the static stiffness was validated with numerical results for clamped–free box-section carbon/epoxy composite beams (e.g. Fig. 3d) having complex circumferentially

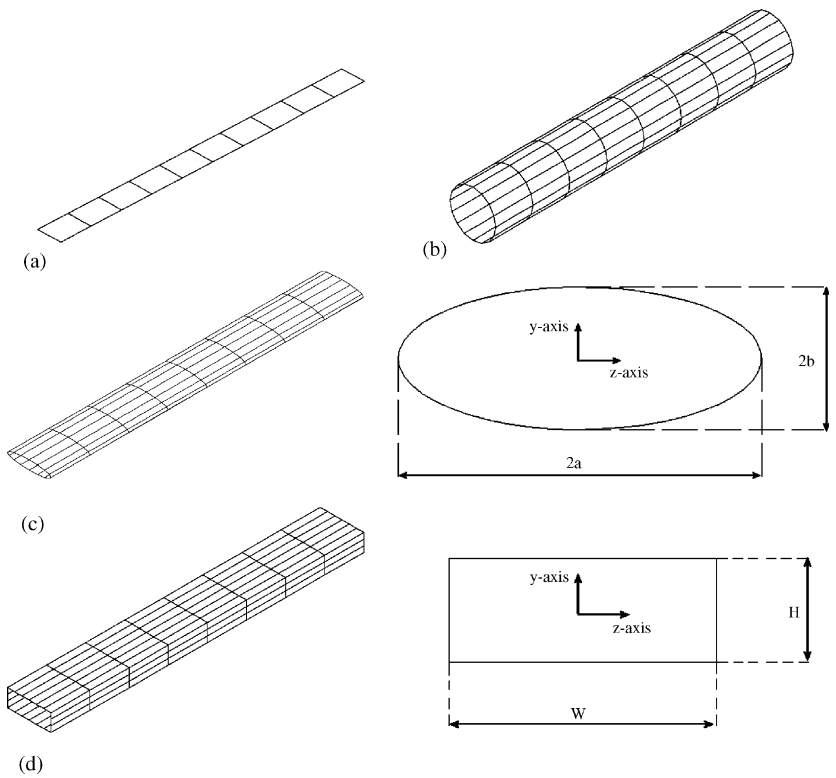

Fig. 3. Beam geometries represented by their skin mid-surface: (a) plate beam, (b) circular section tubular beam, (c) elliptical section tubular blade and (d) box section tubular beam.

Table 1
Mechanical properties of composite material

Ply thickness t_l (mm)	ρ (kg/m^3)	E_{11} (GPa)	E_{22} (GPa)	G_{12} (GPa)	G_{23} (GPa)	v_{12}	η_{l1} (%)	η_{l2} (%)	η_{l4} (%)	η_{l6} (%)
0.635	1672	25.8	8.7	3.5	3.5[a]	0.34	0.65	2.34	2.89[a]	2.89

[a]Not measured.

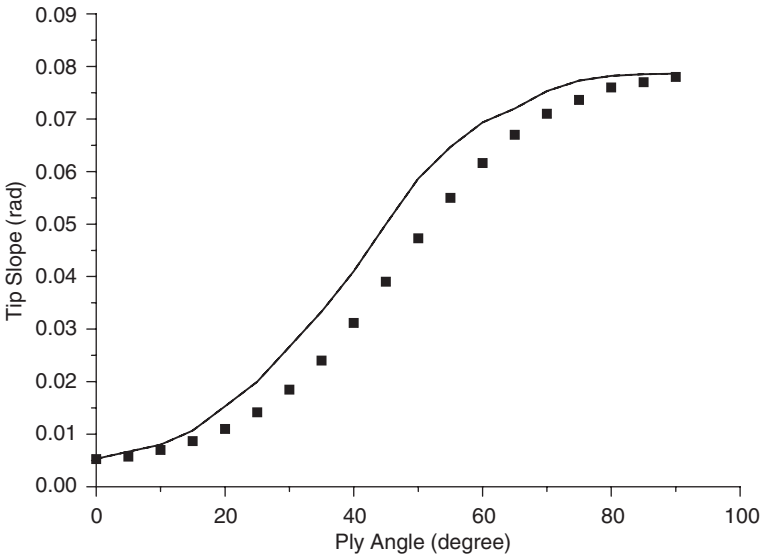

Fig. 4. Tip bending rotation for a clamped–free box section carbon/epoxy beam with $[\theta/-\theta]_3, [-\theta/\theta]_3, [\theta]_6$ and $[-\theta]_6$ skin laminations at the left, right, top and bottom side, respectively. A 4.45 N transverse load was applied at free end. ■ Present FE, ——— Asymptotic [18].

asymmetric section laminations, reported by Volovoi and Hodges [17,18] and were selected to entail various combinations of skin extension–shear, extension–torsion and bending–torsion coupling, as well as, cross-sectional bending coupling. Consequently, the corresponding coupling terms indicated by overbar in the section stiffness matrices shown in Eq. (11) are crucial for these predictions. Fig. 4 shows the predicted tip bending rotation for a section with $[\theta/-\theta]_3$, $[-\theta/\theta]_3$, $[\theta]_6$ and $[-\theta]_6$ skin laminations at the left, right, top and bottom side, respectively [18]. There is a slight underestimation by the present theory in the bending-stiffness prediction, compared with the asymptotic beam theory [17] for ply orientations yielding non-negligible shear–extension coupling, whereas the underestimation vanishes at $\theta = 0^\circ$ and 90°. Fig. 5(a) shows the torsional stiffness of a beam with $[\theta_3/-\theta_3]$ skin laminations at the left and top sides, $[-\theta_3/\theta_3]$ laminations at the right and bottom sides; whereas Fig. 5(b) shows the torsional stiffness of a beam with $[\theta_3/-\theta_3]$ at the left and right sides, and $[-\theta_3/\theta_3]$ at the top and bottom sides [18]. In both cases, the predictions of the present beam theory fall within the range of other theories reported in Ref. [18], and coincide with predictions of beam theories neglecting the presence of hoop bending moments, which apparently underestimate the cross-sectional torsional stiffness for ply orientations yielding strong bending–torsion coupling. However, considering that the present beam model is intended for sections with negligible or minimal bending–torsion damping, its performance in these extreme cases is considered satisfactory. Nevertheless, the proper consideration of shear–extension coupling in the cross-sectional damping and stiffness behavior of tubular beams is intended to be a topic of future research.

4.1. Plate beams

The predicted modal frequencies and damping loss-factors of the first flapwise and edgewise bending modes of cantilever plate beams (Fig. 3a) are shown in Table 2 for various laminations. The beams were 0.32 m wide and had a laminate thickness $L/h = 226$. The current beam element yields excellent correlations of both modal damping and natural frequencies with numerical results predicted by the damped shell finite element [10]. The beam element successfully captures the effect of lamination on bending modal damping. As expected, the predicted modal damping of the [0] and [90] laminate configurations is equal to the longitudinal and transverse loss-factors of the composite material (see Table 1). No torsional modes are shown in Table 2, because the torsional-stiffness formulation assumes closed tubular sections.

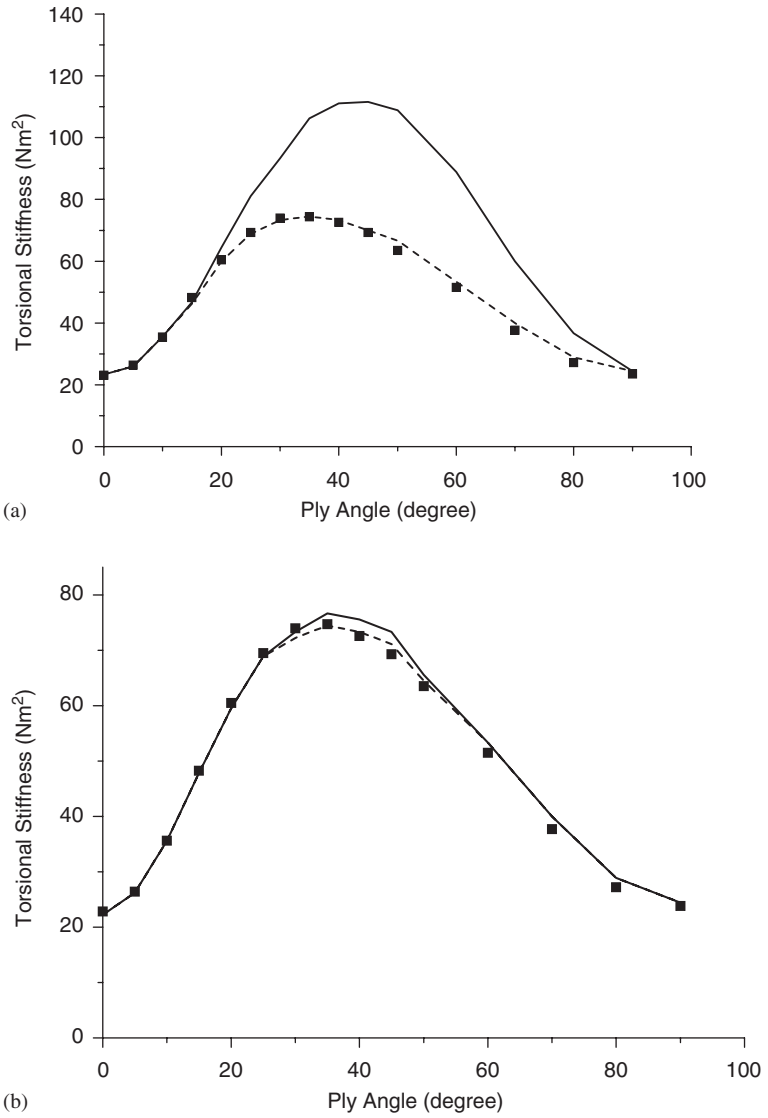

Fig. 5. Tip torsional stiffness of a clamped–free box section carbon/epoxy beam with: (a) $[\theta_3/-\theta_3]$ skin laminations at the left and top side, $[-\theta_3/\theta_3]$ laminations at the right and bottom side; (b) $[\theta_3/-\theta_3]$ at the left and right side, and $[-\theta_3/\theta_3]$ at the top and bottom side. ■ Present FE, ——— Asymptotic [18], – – – – – No hoop moments [18].

4.2. Circular tubular beams

Tubular cantilever beams having circular sections of mid-surface diameter $d = 352\,\text{mm}$ and wall thickness $h = 10.16\,\text{mm}$ were modeled using the current element (Fig. 2b). Table 3 shows the modal damping and frequencies of beams with various skin laminations, all having a length-to-diameter aspect ratio of $L/d = 6.5$; whereas Table 4 shows the predicted modal damping and frequencies for longer beams with length-to-diameter aspect ratio $L/d = 26$. The corresponding predictions using a shell damping theory and damped shell finite element model [10], implementing a 16×8 element mesh along the hoop and axial directions, respectively, are also shown. In all cases, the beam element has seemingly provided excellent predictions of modal damping and modal frequencies. It has successfully captured the effect of skin lamination on the modal damping and frequencies of both bending

Table 2
Modal frequency and damping of laminated plate beams

Lamination	Mode	Natural frequency (Hz)		Loss factor (%)	
		Beam FE	Damped shell FE	Beam FE	Damped shell FE
$[0_8]_s$	First flapping	1.2	1.2	0.645	0.645
	Second flapping	7.8	7.7	0.645	0.646
	First sweeping	37.2	37.3	0.76	0.76
$[90_8]_s$	First flapping	0.7	0.71	2.348	2.348
	Second flapping	4.5	4.5	2.348	2.348
	First sweeping	22.1	22.1	2.357	2.357
$[0_2/90_2/45_2/-45_2]_s$	First flapping	1	1.1	0.953	0.959
	Second flapping	6.7	6.6	0.953	0.960
	First sweeping	28.3	28.5	1.445	1.43
$[45_2/-45_2]_8$	First flapping	0.8	0.8	2.45	2.34
	Second flapping	5	5.0	2.45	2.34
	First sweeping	24.4	24.7	2.434	2.36

Table 3
Modal frequency and damping of various laminated tubular circular beams: $L/d = 6.5$

Lamination	Mode	Natural frequency (Hz)		Loss factor (%)	
		Beam FE	Damped shell FE	Beam FE	Damped shell FE
$[0_8]_s$	First flapping	49.0	46.9	0.84	1.02
	Second flapping	243.6	208.0	1.52	1.86
	First sweeping	49.0	46.9	0.84	1.02
	Second sweeping	243.6	208.0	1.52	1.86
	First torsional	158.0	157.9	2.89	2.89
	Second torsional	474.9	474.2	2.89	2.89
$[90_8]_s$	First flapping	29.4	29.1	2.36	2.37
	Second flapping	164.7	152.3	2.44	2.51
	First sweeping	29.4	29.1	2.36	2.37
	Second sweeping	164.7	152.3	2.44	2.51
	First torsional	157.9	157.9	2.89	2.89
	Second torsional	474.9	474.2	2.89	2.89
$[0_2/90_2/45_2/(-45)_2]_s$	First flapping	37.8	37.2	1.45	1.45
	Second flapping	210.3	194.6	1.47	1.48
	First sweeping	37.8	37.2	1.45	1.45
	Second sweeping	210.3	194.6	1.47	1.48
	First torsional	194.7	196.7	1.60	1.60
	Second torsional	591.5	590.7	1.60	1.60
$[45/-45]_8$	First flapping	32.6	32.5	2.42	2.36
	Second flapping	188.3	181.8	2.29	2.08
	First sweeping	32.6	32.5	2.42	2.36
	Second Sweeping	188.3	181.8	2.29	2.08
	First torsional	228.9	229.0	1.00	0.99
	Second torsional	688.1	687.9	1.00	0.99

and torsional modes. The results highlight the effect of lamination on structural damping, which appears to be very strong.

In addition, the beam element seems to predict the effect of transverse shear on both flexural damping and modal frequencies. This is most apparent in the damping predictions of the shorter ($L/d = 6.5$) beam

Table 4
Modal frequency and damping of various laminated tubular circular beams: $L/d = 26$

Lamination	Mode	Natural frequency (Hz)		Loss factor (%)	
		Beam FE	Damped shell FE	Beam FE	Damped shell FE
$[0_8]_s$	First flapping	3.2	3.2	0.66	0.70
	Second flapping	19.9	19.5	0.74	0.84
	First sweeping	3.2	3.2	0.66	0.70
	Second sweeping	19.9	19.5	0.74	0.84
	First torsional	39.5	39.5	2.89	2.89
	Second torsional	118.7	118.4	2.89	2.89
$[90_8]_s$	First flapping	1.9	2.0	2.35	2.17
	Second flapping	11.7	11.9	2.36	2.30
	First sweeping	1.9	2.0	2.35	2.17
	Second sweeping	11.7	11.9	2.36	2.30
	First torsional	39.5	39.5	2.89	2.89
	Second torsional	118.7	118.4	2.89	2.89
$[0_2/90_2/45_2/(-45)_2]_s$	First flapping	2.4	2.5	1.44	1.44
	Second flapping	15.0	15.1	1.44	1.45
	First sweeping	2.4	2.5	1.44	1.44
	Second sweeping	15.0	15.1	1.44	1.45
	First torsional	49.2	49.2	1.60	1.60
	Second torsional	148.0	147.5	1.60	1.60
$[45/-45]_8$	First flapping	2.0	2.1	2.45	2.39
	Second flapping	13.0	13.1	2.44	2.39
	First sweeping	2.0	2.1	2.45	2.39
	Second sweeping	13.0	13.1	2.44	2.39
	First torsional	57.0	57.3	1.00	0.99
	Second torsional	172.0	171.8	1.00	0.99

for skin laminations yielding low transverse shear stiffness ($[0]_{16}$ and $[0/90/45]_s$), where the damping predictions for the bending modes, although in good agreement with those of the shell element, substantially exceed the flexural damping loss factors of the thin plate beam. Table 5 shows predicted damping and frequency values for the first bending and torsion mode of circular beams with various aspect ratios (L/d), and quantifies the capability of the beam element to capture transverse shear damping contributions at low L/d aspect ratios. As the aspect ratio L/d increases, the contribution of shear damping is progressively reduced; in the latter case, the damping and frequencies predicted by the beam element includes mainly contributions from flexural damping and stiffness components. Conversely, the results also quantify the underestimation in damping predictions of a classical beam element neglecting shear vs. the present shear beam. Overall, there is very good agreement between the damping predictions of the present beam element and those of the shell-theory-based element; moreover, the present beam element seems to provide robust predictions for a wide range of length aspect ratios. Any differences in the damping and frequency predictions between the beam and shell elements at low L/d ratios are mostly attributed to the constant shear strain assumption, as well as, to deviations of the beam deformation from the assumed kinematic assumptions of the beam element. It is recalled that the previous results were achieved without considering any shear correction factors in the through-the-thickness integration of the shear strain-energy term in Eq. (10). Hence, it seems likely that shear correction factors may be estimated, which upon implementation into Eq. (10) may further improve the agreement between the present beam element and the shell element at low L/d ratios; however, the proper selection and effectiveness of such shear correction factors remains a topic of future studies.

Table 5
Effect of length aspect ratio L/d on modal damping of circular tubular composite beams

Lamination	Modal frequency (Hz)				Modal loss-factor (%)			
	First flapping		First twisting		First flapping		First twisting	
	Beam	Shell	Beam	Shell	Beam	Shell	Beam	Shell
$[0]_{16}$								
$L/d = 6.5$	49.0	46.9	158.0	157.9	0.85	1.02	2.89	2.89
13	12.8	12.7	79.0	78.9	0.70	0.78	2.89	2.89
26	3.2	3.2	39.5	39.5	0.66	0.70	2.89	2.89
104	0.20	—	9.9	—	0.65	—	2.89	—
$[90]_{16}$								
$L/d = 6.5$	29.4	29.1	158.0	157.9	2.37	2.37	2.89	2.89
13	7.5	7.9	79.0	78.9	2.35	2.25	2.89	2.89
26	1.9	2.0	39.5	39.5	2.35	2.17	2.89	2.89
104	0.12	—	9.9	—	2.35	—	2.89	—
$[0_2/90_2/45_2/-45_2]_s$								
$L/d = 6.5$	37.7	37.2	196.8	196.7	1.45	1.45	1.60	1.60
13	9.6	9.8	98.4	98.3	1.44	1.45	1.60	1.60
26	2.4	2.5	49.2	49.2	1.44	1.44	1.60	1.60
104	0.15	—	12.3	—	1.44	—	1.60	—
$[45/-45]_8$								
$L/d = 6.5$	32.6	32.5	228.9	229.0	2.42	2.36	1.00	0.99
13	8.3	8.5	114.5	114.5	2.44	2.39	1.00	0.99
26	2.0	2.1	57.2	57.3	2.45	2.39	1.00	0.99
104	0.13	—	14.3	—	2.45	—	1.00	—

4.3. Elliptical cross-section blade

An elliptical cross-section blade was considered clamped at one end, as shown in Fig. 3c. The semi-major axis of the section is $a = 0.16$ m, the major to minor semi-axis ratio $a/b = 4.85$, and the wall thickness $h = 10.16$ mm. The predicted modal damping and natural frequency of an elliptical beam of length ratio $L/2a = 7.2$ are shown in Table 6. There is very good agreement between the damping and frequencies predicted by the beam element and those predicted by the shell element. As in the previous cases, the results show the predominant effect of skin lamination on the modal damping of the beam, which varies widely between flapping, sweeping and torsional mode shapes. In addition, the beam element seems to have successfully captured the effect of cross-section geometry on both damping and frequencies, as indicated by the differences in modal frequency predictions between flapping and sweeping modes. The predicted effect of the semi-axis ratio a/b on the fundamental modes is further illustrated in Table 7. Clearly, the predicted transverse shear damping contributions may vary widely depending on cross-sectional shape and laminate configuration. Predicted modal damping and frequency values of blades of various length aspect ratios $L/2a$ are shown in Table 8. Tables 6–8 also demonstrate the capability of the present beam element to capture effects of transverse shear on the modal damping and frequencies of the blade, and the same comments described in the circular beam case apply also here. Overall, the results illustrate that the present beam element yields very good and robust damping and frequency predictions for elliptical section blades, whereas, its accuracy progressively improves at high length aspect ratios.

4.4. Box-section beams

Cantilever rectangular box-section beams were also analyzed using the present beam element. Table 9 shows predicted modal damping and frequency values of beams having a square cross-section with $w = 0.32$ m

Table 6
Modal frequencies and damping of an elliptical tubular beam for various skin laminate configurations; $L/2a = 7.2$, $a/b = 4.85$

Lamination	Mode	Natural frequency (Hz)		Loss factor (%)	
		Beam FE	Damped shell FE	Beam FE	Damped shell FE
$[0_8]_S$	First flapping	11.0	10.8	0.66	0.85
	Second flapping	68.3	58.2	0.71	1.37
	First sweeping	38.6	38.6	0.77	0.80
	Second sweeping	207.1	201.8	1.28	1.37
	First torsional	78.7	76.0	2.89	2.81
	Second torsional	236.5	177.8	2.89	2.56
$[90_8]_S$	First flapping	6.4	6.7	2.35	2.36
	Second flapping	40.2	39.2	2.35	2.42
	First sweeping	22.9	23.3	2.36	2.33
	Second sweeping	133.7	133.6	2.41	2.41
	First torsional	78.7	77.5	2.89	2.82
	Second torsional	236.5	210.8	2.89	2.40
$[0_2/90_2/45_2/(-45)_2]_S$	First flapping	8.3	8.5	1.44	1.47
	Second flapping	51.7	49.7	1.44	1.47
	First sweeping	29.4	29.6	1.45	1.45
	Second sweeping	171.1	169.9	1.46	1.46
	First torsional	97.8	94.1	1.61	1.59
	Second torsional	294.2	220.6	1.61	1.51
$[45/-45]_8$	First flapping	7.1	7.5	2.44	2.31
	Second flapping	44.3	44.9	2.44	2.20
	First sweeping	25.3	25.6	2.43	2.39
	Second sweeping	150.8	151.2	2.34	2.29
	First torsional	114.0	107.7	1.00	1.06
	Second torsional	342.7	232.9	1.00	1.37

Table 7
Effect of section aspect ratio a/b on modal characteristics of elliptical tubular composite beams: $L/2a = 7.2$

Laminate	Modal frequency (Hz)						Modal loss-factor (%)					
	First flap		First sweep		First twist		First flap		First sweep		First twist	
	Beam	Shell	Beam	Shell	Beam	Shell	Beam	Shell	Beam	Shell	Beam	Shell
$[0]_{16}$												
$a/b = 10$	4.5	—	39.3	—	25.8	—	0.65	—	0.77	—	2.85	—
7.5	7.2	—	37.9	—	54.7	—	0.65	—	0.76	—	2.89	—
5.0	11.0	10.8	38.6	38.6	78.7	76.0	0.66	0.85	0.77	0.80	2.89	2.81
2.5	21.0	20.3	40.6	40.4	124.8	116.7	0.68	0.83	0.78	0.83	2.89	2.77
1.0	44.9	43.3	44.9	43.3	158	157.9	0.81	0.96	0.81	0.96	2.89	2.89
$[0_2/90_2/45_2/-45_2]_s$												
$a/b = 10$	3.4	—	30.0	—	31.6	—	1.40	—	1.45	—	1.69	—
7.5	5.4	—	28.8	—	67.9	—	1.43	—	1.45	—	1.62	—
5.0	8.3	8.5	29.4	29.6	97.9	94.1	1.44	1.47	1.45	1.47	1.61	1.59
2.5	15.8	15.7	31.0	31.0	155.4	145.5	1.44	1.44	1.45	1.44	1.60	1.56
1.0	34.4	34.0	34.4	34.0	196.8	196.7	1.45	1.44	1.45	1.44	1.60	1.60

wide flanges, flange width-to-web thickness ratio $w/H = 5$, length ratio $L/w = 14.37$, skin thickness $h = 10.16$ mm, and various skin laminations. Predictions of modal frequencies using a commercially available eight-node shell element [21] are also shown. Table 10 shows the effect of section aspect ratio

Table 8
Effect of length aspect ratio L/a on modal damping and frequencies of elliptical tubular composite beams predicted using the present beam element: $a/b = 4.85$

Laminate	Modal frequency (Hz)			Modal loss-factor (%)		
	First flapping	First sweeping	First twisting	First flapping	First sweeping	First twisting
$[0]_{16}$						
$L/2a = 7.2$	11.0	38.5	78.7	0.66	0.77	2.89
14.4	2.8	9.9	39.3	0.65	0.68	2.89
28.8	0.7	2.5	19.7	0.65	0.65	2.89
115.2	0.04	0.15	4.90	0.65	0.65	2.89
$[90]_{16}$						
$L/2a = 7.2$	6.4	22.9	78.7	2.35	2.36	2.89
14.4	1.6	5.8	39.3	2.35	2.35	2.89
28.8	0.4	1.5	19.7	2.35	2.35	2.89
115.2	0.02	0.09	4.90	2.35	2.35	2.89
$[0_2/90_2/45_2/-45_2]_s$						
$L/2a = 7.2$	8.3	29.4	97.8	1.44	1.45	1.61
14.4	2.1	7.4	48.9	1.44	1.44	1.61
28.8	0.5	1.9	24.5	1.44	1.44	1.61
115.2	0.03	0.11	6.1	1.44	1.44	1.61
$[45/-45]_8$						
$L/2a = 7.2$	7.1	25.3	114.0	2.44	2.43	1.0
14.4	1.8	6.4	57.0	2.45	2.44	1.0
28.8	0.4	1.6	28.5	2.45	2.45	1.0
115.2	0.03	0.1	7.12	2.45	2.45	1.0

w/H on fundamental modal damping and frequencies, while Table 11 shows the effect of beam length aspect ratio L/w on the modal characteristics. As in the previous cases, the beam element has captured the effect of section lamination and cross-sectional geometry on both structural damping and frequencies. The beam element seems to capture transverse shear damping contributions on the overall damping of the box beam, and most previous comments of the circular and elliptical sections seem to apply here. The deviation at the second torsional frequency may be attributed to local hoop warping observed in the shell FE model, which may not be fully accounted by the present beam model.

Overall, all previous studies demonstrate that the developed shear damping beam theory and beam element have provided accurate and computationally efficient modal damping, modal frequency and mode shape predictions in composite beams and blades of various skin laminate configuration and cross-sectional shape, while it can robustly predict damping and frequencies in both short and long beams and blades. It is pointed out, however, that the considered laminate configurations exhibit negligible extension–shear coupling in both stiffness and damping. Laminate and/or section configurations exhibiting strong extension–shear or other forms of laminate coupling may involve additional damping terms and may yield different structural damping. Yet, their analysis requires additional consideration which exceeds the scope of the present paper, thus, they will be investigated in the near future.

5. Summary and conclusions

An integrated damping mechanics formulation for composite tubular beams and blades including transverse shear effects was presented. A shear beam element was further developed encompassing unique capabilities to predict the damping, stiffness and mass matrices of the blade, as well as, to provide the damped modal characteristics and the damped vibration response. As a result of the integrated formulation, the beam

Table 9
Modal frequencies and damping of a box-section beam for various skin laminate configurations: $L/w = 14.36$, $w/H = 5$

Lamination	Mode	Modal loss-factor (%)	Modal frequency (Hz)	
		Beam FE	Beam FE	Commercial shell FE [21]
$[0]_{16}$				
	First flapping	0.65	3.1	3.1
	Second flapping	0.67	19.8	18.5
	First sweeping	0.68	11.0	10.9
	Second sweeping	0.9	65.6	63.9
	First torsional	2.89	37.7	37.0
	Second torsional	2.89	113.3	93.7
$[90]_{16}$				
	First flapping	2.35	1.8	1.8
	Second flapping	2.35	11.5	11.2
	First sweeping	2.35	6.5	6.4
	Second sweeping	2.37	39.7	39.1
	First torsional	2.89	37.7	37.5
	Second torsional	2.89	113.3	105.1
$[0_2/90_2/45_2/-45_2]_s$				
	First flapping	1.44	2.4	2.4
	Second flapping	1.44	14.8	14.5
	First sweeping	1.44	8.3	8.3
	Second sweeping	1.45	50.9	50.3
	First torsional	1.61	46.9	45.9
	Second torsional	1.61	140.9	116.3
$[45/-45]_8$				
	First flapping	2.45	2.0	2.03
	Second flapping	2.45	12.7	12.6
	First sweeping	2.45	7.1	7.2
	Second sweeping	2.41	44.1	44.0
	First torsional	0.99	54.6	52.9
	Second torsional	0.99	164.2	125.8

requires minimal input of material and blade geometry data. The described mechanics and the finite element were encoded into a research finite element code, named DAMPBEAM, which enables the prediction of the damped modal characteristics of the blade.

Numerous successful validations and evaluations of the damped beam element were presented for laminated glass/polyester composite beams of circular, elliptical and box sections having various laminate configurations exhibiting negligible extension–shear coupling in stiffness and damping. The developed damping beam theory and the beam element have provided accurate and computationally efficient modal damping, modal frequency and mode shape predictions in composite beams and blades of various cross-sections and lengths. The beam element has successfully captured the effects of skin laminate configuration on structural damping. Moreover, the beam element clearly entails the capability to capture transverse shear effects, thus robustly predicting damping and frequencies in both short and long beams and blades. Overall, the shear beam element seems to combine the capacity to yield accurate and robust predictions of the damped structural response of composite blades, thus providing a valuable analytical tool for the design and aeroelastic analysis of either wind-turbine or helicopter rotor blades.

Future work will be directed towards the study of laminate and/or section configurations exhibiting strong extension–shear or other forms of coupling, as well as, towards the correlation of beam element results with measured modal data on model airfoil blades.

Table 10
Effect of box section aspect ratio w/H on modal damping of composite beams: $L/w = 14.36$

Lamination	Modal frequency (Hz)			Modal loss-factor (%)		
	First flap	First sweep	First twist	First flap	First sweep	First twist
$[0]_{16}$						
$w/H = 10$	1.6	10.4	22.5	0.64	0.68	2.89
7.5	2.1	10.6	28.1	0.64	0.68	2.89
5	3.1	11.0	37.7	0.65	0.68	2.89
2.5	6.0	11.9	55.7	0.65	0.69	2.89
1	13.4	13.4	67.8	0.7	0.7	2.89
$[90]_{16}$						
$w/H = 10$	0.9	6.1	22.5	2.35	2.36	2.89
7.5	1.2	6.2	28.1	2.35	2.35	2.89
5	1.8	6.5	37.7	2.35	2.35	2.89
2.5	3.5	7.0	55.6	2.35	2.35	2.89
1	7.9	7.9	67.9	2.35	2.35	2.89
$[0_2/90_2/45_2/-45_2]_s$						
$w/H = 10$	1.2	7.8	27.9	1.42	1.44	1.62
7.5	1.6	8.0	34.9	1.43	1.44	1.61
5	2.4	8.3	46.9	1.44	1.44	1.61
2.5	4.5	9.0	69.3	1.44	1.44	1.60
1	10.1	10.1	84.5	1.44	1.44	1.60
$[45/-45]_8$						
$w/H = 10$	1.0	6.7	32.6	2.45	2.44	0.99
7.5	1.3	8.6	40.7	2.45	2.45	0.99
5	2.0	7.1	54.6	2.45	2.45	0.99
2.5	3.8	7.7	80.6	2.45	2.44	0.99
1	8.7	8.7	98.3	2.44	2.44	0.99

Table 11
Effect of length aspect ratio on modal damping of box section composite beams: $w/H = 5$

Lamination	Modal frequency (Hz)			Modal loss-factor (%)		
	First flap	First sweep	First twist	First flap	First sweep	First twist
$[0]_{16}$						
$L/w = 7.187$	12.5	42.8	75.3	0.66	0.80	2.89
14.37	3.1	11.0	37.7	0.65	0.68	2.89
28.75	0.8	2.8	18.8	0.64	0.65	2.89
115	0.05	0.18	4.7	0.64	0.64	2.89
$[90]_{16}$						
$L/w = 7.187$	7.3	25.5	75.3	2.35	2.36	2.89
14.37	1.8	6.5	37.7	2.35	2.35	2.89
28.75	0.4	1.6	18.8	2.35	2.35	2.89
115	0.03	0.1	4.7	2.35	2.35	2.89
$[0_2/90_2/45_2/-45_2]_s$						
$L/w = 7.187$	9.4	32.7	93.7	1.44	1.44	1.60
14.37	2.4	8.3	46.9	1.44	1.44	1.60
28.75	0.6	2.0	23.4	1.44	1.44	1.60
115	0.04	0.13	5.8	1.44	1.44	1.60
$[45/-45]_8$						
$L/w = 7.187$	8.0	28.2	109.2	2.45	2.43	0.99
14.37	2.0	7.1	54.6	2.45	2.45	0.99
28.75	0.5	1.8	27.3	2.45	2.45	0.99
115	0.03	0.1	6.8	2.45	2.45	0.99

Acknowledgments

This work was supported by the 5th EU Research Framework under the DAMPBLADE ENK6-CT2000-00320 ENERGIE project. This financial support is gratefully acknowledged by the authors.

Appendix A

A.1. Ply damping

The dissipated energy per unit volume per cycle within a ply is given by the following form:

$$W_c = \tfrac{1}{2}\boldsymbol{\varepsilon}_c^{\mathrm{T}}\boldsymbol{\eta}_c\mathbf{Q}_c\boldsymbol{\varepsilon}_c = \tfrac{1}{2}\boldsymbol{\sigma}_c^{\mathrm{T}}\mathbf{S}_c\boldsymbol{\eta}_c\boldsymbol{\sigma}_c, \tag{28}$$

where $\mathbf{Q}_c$ is the ply stiffness matrix in the local skin coordinates $xs\zeta$ of the beam section, $\mathbf{S}_c$ is the ply compliance matrix, $\boldsymbol{\sigma}_c$ is the maximum cyclic stress, and $\boldsymbol{\eta}_c$ is the off-axis damping matrix related to on-axis damping coefficients by the relation

$$\boldsymbol{\eta}_c = \mathbf{R}^{-1}\boldsymbol{\eta}_l\mathbf{R}, \tag{29}$$

where $\mathbf{R}$ is proper rotation matrix, $\boldsymbol{\eta}_l$ is the damping matrix at the material coordinate system $O123$ (1—longitudinal, 2—transverse, and 3—through-thickness axes) having the following diagonal form [3]:

$$\boldsymbol{\eta}_l = \mathbf{diag}(\eta_{l1}, \eta_{l2}, \eta_{l4}, \eta_{l5}, \eta_{l6}), \tag{30}$$

where η_{l1} is the longitudinal damping (direction 11), η_{l2} is the transverse in-plane damping (direction 22), η_{l6} is the in plane shear damping (direction 12), η_{l4} is the interlaminar shear damping (direction 23), and $\eta_{l5} = \eta_{l6}$ are the interlaminar shear damping (direction 13). These on-axis damping values are used as input for the calculation of the beam damping.

A.1.1. Skin laminate damping and stiffness matrices

The membrane, coupling and flexural damping and stiffness matrices of the skin laminate are calculated based on first-order shear theory assumptions [10]. For example, the damping matrices have the form

$$\langle A_{d_{ij}}, B_{d_{ij}}, D_{d_{ij}}\rangle = \int_{-h/2}^{h/2} \eta_{c_{ik}} Q_{c_{kj}} \langle 1, \zeta, \zeta^2\rangle \,\mathrm{d}\zeta, \quad i,j,k = 1,2,6,$$

$$\langle A_{d_{ij}}\rangle = \int_{-h/2}^{h/2} \eta_{c_{ik}} Q_{c_{kj}} \,\mathrm{d}\zeta, \quad i,j,k = 4,5. \tag{31}$$

A.1.2. Reduced skin laminate matrices

The laminate stiffness and damping matrices are further reduced, assuming that the equivalent hoop force, moment and shear force, N_s, M_s and $N_{\zeta s}$, respectively, defined with respect to the local section coordinates $xs\zeta$, should be negligible. If $\mathbf{C}_L$ and $\mathbf{C}_{dL}$ are the laminate stiffness and damping matrices

$$\mathbf{C}_L = \begin{bmatrix} \mathbf{A} & \mathbf{B} \\ \mathbf{B}^{\mathrm{T}} & \mathbf{D} \end{bmatrix}, \quad \mathbf{C}_{dL} = \begin{bmatrix} \mathbf{A}_d & \mathbf{B}_d \\ \mathbf{B}_d^{\mathrm{T}} & \mathbf{D}_d \end{bmatrix} \tag{32}$$

then their respective compliance counterparts are $\mathbf{S}_L = \mathbf{C}_L^{-1}$ and $\mathbf{S}_{dL} = \mathbf{S}_L^{\mathrm{T}}\mathbf{C}_{dL}\mathbf{S}_L$. Then,

$$\delta H_L = \{\delta\mathbf{N}, \delta\mathbf{M}\}^{\mathrm{T}}\mathbf{S}_L\begin{Bmatrix}\mathbf{N}\\ \mathbf{M}\end{Bmatrix} = \{\delta\mathbf{N}^*, \delta\mathbf{M}^*\}^{\mathrm{T}}\mathbf{S}_L^*\begin{Bmatrix}\mathbf{N}^*\\ \mathbf{M}^*\end{Bmatrix}, \tag{33}$$

$$\delta W_{dL} = \{\delta\mathbf{N}, \delta\mathbf{M}\}^{\mathrm{T}}\mathbf{S}_{dL}\begin{Bmatrix}\mathbf{N}\\ \mathbf{M}\end{Bmatrix} = \{\delta\mathbf{N}^*, \delta\mathbf{M}^*\}^{\mathrm{T}}\mathbf{S}_{dL}^*\begin{Bmatrix}\mathbf{N}^*\\ \mathbf{M}^*\end{Bmatrix}. \tag{34}$$

Superscript L indicates the skin laminate, $\mathbf{N}$ and $\mathbf{M}$ are effective laminates average stress and moment vectors. The star superscript indicates the resultant reduced forces and matrices, after the application of the zero hoop force and moment assumption $N_s = M_s = N_{\zeta s} = 0$. Hence, the reduced laminate damping and stiffness matrices take the form

$$\mathbf{C}_L^* = \mathbf{S}_L^{*^{-1}}, \quad \mathbf{C}_{dL}^* = \mathbf{C}_L^{*^{\mathrm{T}}} \mathbf{S}_{dL}^* \mathbf{C}_L^* \tag{35}$$

and contain the reduced membrane, coupling and flexural stiffness and damping matrices used in the calculation of the sectional matrices. For example,

$$\mathbf{A}^* = \begin{bmatrix} A_{11}^* & 0 & A_{61}^* \\ 0 & A_{55}^* & 0 \\ A_{16}^* & 0 & A_{66}^* \end{bmatrix}, \quad \mathbf{B}^* = \begin{bmatrix} B_{11}^* & B_{61}^* \\ B_{16}^* & B_{66}^* \end{bmatrix}, \quad \mathbf{D}^* = \begin{bmatrix} D_{11}^* & D_{61}^* \\ D_{16}^* & D_{66}^* \end{bmatrix}. \tag{36}$$

The corresponding damping matrices $\mathbf{A}_d^*$, $\mathbf{B}_d^*$, $\mathbf{D}_d^*$ have similar form. The asterisk superscript is implied in Eqs. (12)–(14) and (20)–(22).

A.1.3. Skin laminate densities

$$\langle \rho^A, \rho^B, \rho^D \rangle = \int_{-h/2}^{h/2} \rho \langle 1, \zeta, \zeta^2 \rangle \mathrm{d}\zeta, \tag{37}$$

where ρ is the ply density, ζ is the distance from the skin midline.

A.1.4. Finite element matrices

The element stiffness matrix including in-plane and shear terms is

$$\mathbf{K}_e^{ij} = \int_0^L \mathbf{R}^{i^{\mathrm{T}}} \begin{bmatrix} \mathbf{A}^0 & \mathbf{B}^0 \\ \mathbf{B}^{0^{\mathrm{T}}} & \mathbf{D}^0 \end{bmatrix} \mathbf{R}^j \, \mathrm{d}x \tag{38}$$

and the element mass matrix l contains terms of linear density, rotational and polar inertia, and coupling terms of the section through the relation

$$\mathbf{M}_e^{ij} = \int_0^L \mathbf{N}^{i^{\mathrm{T}}} \begin{bmatrix} \boldsymbol{\rho}^{\mathbf{A}} & \boldsymbol{\rho}^{\mathbf{B}} \\ \boldsymbol{\rho}^{\mathbf{B}^{\mathrm{T}}} & \boldsymbol{\rho}^{\mathbf{D}} \end{bmatrix} \mathbf{N}^j \, \mathrm{d}x. \tag{39}$$

References

[1] R.G. Ni, R.D. Adams, The damping and dynamic moduli of symmetric laminated composite beams—theoretical and experimental results, *Journal of Composite Materials* 18 (2) (1984) 104–121.

[2] R.F. Gibson, R. Plunkett, Dynamic mechanical behaviour of fiber-reinforced composites: measurements and analysis, *Journal of Composite Materials* 10 (1976) 325–341.

[3] D.A. Saravanos, C.C. Chamis, Mechanics of damping for fiber composite laminates including hygro-thermal effects, *American Institute of Aeronautics and Astronautics Journal* 28 (10) (1990) 1813–1819.

[4] C.G. Wren, V.K. Kinra, Axial damping in metal–matrix composites, I: a theoretical model and its experimental verification, *Experimental Mechanics* 32 (2) (1992) 172–178.

[5] S. Bicos, G.S. Springer, Vibrational characteristics of composite panels with cutouts, *American Institute of Aeronautics and Astronautics Journal* 27 (8) (1989) 1116–1122.

[6] N. Alam, N.T. Asnani, Vibration and damping analysis of fibre reinforced composite material plates, *Journal of Composite Materials* 20 (1) (1986) 2–18.

[7] D.A. Saravanos, C.C. Chamis, Computational simulation of damping in composite structures, *Journal of Reinforced Plastics and Composites* 10 (3) (1991) 256–278.

[8] D.A. Saravanos, Analysis of passive damping in thick composite structures, *American Institute of Aeronautics and Astronautics Journal* 31 (8) (1993) 1503–1510.

[9] S.P. Singh, K. Gupta, Damped free vibrations of layered composite cylindrical shells, *Journal of Sound and Vibration* 172 (2) (1994) 191–209.

[10] T.S. Plagianakos, D.A. Saravanos, Mechanics and finite elements for the damped dynamic characteristics of curvilinear laminates and composite shell structures, *Journal of Sound and Vibration* 263 (2) (2003) 399–414.

[11] J.B. Kosmatka, On the behaviour of pretwisted beams with irregular cross sections, *Journal of Applied Mechanics* 59 (1) (1992) 146–152.
[12] R. Chandra, I. Copra, Experimental–theoretical investigation of the vibration characteristics of rotating composite box beams, *Journal of Aircraft* 29 (3) (1992) 657–664.
[13] D.L. Kunz, Survey and comparison of engineering beam theories for helicopter rotor blades, *Journal of Aircraft* 31 (3) (1994) 473–479.
[14] C.E.S. Cesnik, D.H. Hodges, Cross-sectional analysis of composite beams including large initial twist and curvature effects, *American Institute of Aeronautics and Astronautics Journal* 34 (9) (1996) 1913–1920.
[15] O. Song, N.H. Jeong, L. Librescu, Vibration and stability of pretwisted spinning thin-walled composite beams featuring bending–bending elastic coupling, *Journal of Sound and Vibration* 237 (3) (2000) 513–533.
[16] W. Yu, D.H. Hodges, V.V. Volovoi, C.E.S. Cesnik, On Timoshenko-like modeling of initially curved and twisted composite beams, *International Journal of Solids and Structures* 39 (19) (2002) 5101–5121.
[17] V.V. Volovoi, D.H. Hodges, Theory of anisotropic thin-walled beams, *Journal of Applied Mechanics* 67 (3) (2000) 453–459.
[18] V.V. Volovoi, D.H. Hodges, Single and multi-celled composite thin-walled beams, *AIAA Journal* 40 (5) (2002) 960–965.
[19] S.Y. Oh, O. Song, L. Librescu, Effects of pretwist and presetting on coupled bending vibrations of rotating thin-walled composite beams, *International Journal of Solids and Structures* 40 (5) (2003) 1203–1224.
[20] N. Chrisochoidis, Measurement of Damping Coefficients of Glass/Polyester Composites, MS Thesis, Department of Mechanical Engineering and Aeronautics, University of Patras, Greece, 2001.
[21] MSC/NASTRAN Installation and Application Manual, McNeal–Schwendler Corporation, Los Angeles, 1998.